Arch. Metall. Mater. **68** (2023), 1, 275-286

DOI: https://doi.org/10.24425/amm.2023.141504

HANG SHANG[1,2], QIUZHI GAO[1,2*], YUJIAO JIANG[1,2],
QINGSHUANG MA[1,2], HUIJUN LI[3*], HAILIAN ZHANG[4*]

INTERFACE DIFFUSION BEHAVIOR OF Co40Al-X (X = Ni, Cr, Ti) SYSTEM BY DIFFUSION MULTIPLE

Diffusion multiple method was applied to investigate the alloying elements distribution and interface diffusion reactions in Co-Al-X system, in order to accelerate the alloy development. The diffusion regions of Co-Al-X system at 1173 K were investigated by scanning electron microscope (SEM) and nanoindentation. SEM images show that phases of Co-Al-Ni diffusion interface consisted of β-CoAl + γ_{Co}, γ_{Co}, $\gamma + \gamma'$-(Co, Ni)$_3$Al and γ_{Ni}, while Co-Al-Cr diffusion interface is shaped with $\delta + \gamma + \beta$, γ and σ region. $TiNi_X$ diffusion layer with high Ni-content was formed in Co-Al-Ti diffusion interface. The diffusion layers during diffusion multiple play an important role in mechanical properties in these alloying systems. The $\gamma + \gamma'$ diffusion layer in Co-Al-Ni diffusion interface presented the best comprehensive performance, while the highest hardness (17.48 GPa) was confirmed in Co-Al-Cr diffusion interface due to a large number of brittle phases. Darken method was applied to determine the interdiffusion coefficients of alloying elements in pseudo-binary phase, accordingly the diffusion capacities of alloying elements can be ordered as Al > Ni > Cr in Co-based alloys.

Keywords: Co-Al-X system; diffusion multiple; interface; diffusion; mechanical properties

1. Introduction

Diffusion multiple is an assembly of several block metals in a predetermined way to form various binary diffusion couples and ternary diffusion joints [1,2]. The high-throughput diffusion multiple approach has been widely used to create compositional variations of solid solutions and intermetallics with aim of alloys designing. Compared with traditional "Cooking" methods, the diffusion multiple represents distinctive advantages to give effective information about the diffusion mechanism of elements and determining thermodynamic database [3], which is employed to design and screen new materials in recent years [4].

Strengthened by the γ'-$Co_3(Al,W)$ phase with an ordered $L1_2$ structure, Co-based superalloys [5] possesses higher temperature strength compared to conventional Co-based alloys. Alloying elements in Co-based superalloys is a key factor to adjust the strengthening effect of secondary phases (precipitates) [6]. Up to now, many efforts have been focused on the partitioning tendency of elements in intermediate compounds of Co-Al-X system. Omori et al. [7] studied the partitioning behavior of alloying elements in Co-Al-W-based quaternary systems and showed that Ta, Nb, Ti, V, Mo and W elements are partitioned into γ' phase rather than γ phase, which can improve the thermal stability of γ' phase [8]. Yuan et al. [2,9] reported interfacial diffusion of Co-Ni-Ti and Co-Ni-Fe systems under 1173 K, and calculated the diffusion coefficients at this temperature. However, there are few reports on elements variations in W-free Co-Al-X diffusion interface.

Phase composition plays a vital role in the performances of W-free Co-based system, which is a key factor for designing alloys with excellent properties [10]. It has been reported additions of Ni and Ti elements in Co-Al-X alloys can not only strengthen the microstructure but also stabilize γ phase and γ' phase [11-14]. However, it should be noted that excess addition of Ti increases the tendency of Ni_3Ti formation which could result in the alloy brittleness [15]. Similarly, the addition of Cr element can enhance mechanical properties and oxidation resistance of alloys, but excess Cr will increase the formation of TCP phase leading to increased brittleness of alloys [16-23]. Based on our previous studies about the effect of Cr or Mo in Co-Ni-Al-Ti superalloy system on the microstructure and mechanical properties [24], to better understand the reaction mechanisms of different alloying

[1] NORTHEASTERN UNIVERSITY AT QINHUANGDAO, SCHOOL OF RESOURCES AND MATERIALS, QINHUANGDAO, 066004, CHINA
[2] NORTHEASTERN UNIVERSITY, SHENYANG, SCHOOL OF MATERIALS SCIENCE AND ENGINEERING, 110819, CHINA
[3] TIANJIN UNIVERSITY, SCHOOL OF MATERIALS SCIENCE & ENGINEERING, TIANJIN, 300354, CHINA
[4] DAOTIAN HIGH TECHNOLOGY CO., LTD., QINHUANGDAO, 066004, CHINA

* Corresponding author: neuqgao@163.com; huijun@uow.edu.au; hailianchina@126.com

elements, herein, this work investigated the effect of other alloying elements (Ni, Cr, Ti) on microstructure evolution of W-free Co-Al based system, formation of intermetallic compounds and application of the elements reactions. Specifically, by applying diffusion multiple, the diffusion behavior of Co-Al-Ni, Co-Al-Cr and Co-Al-Ti ternary systems was studied, and diffusion abilities of various elements as well as the mechanical properties of various diffusion layers were also discussed.

2. Experimental procedures

2.1. Experiments

The diffusion multiple technique was used to determine the isothermal sections of Co-Al-X (X = Ni, Cr, Ti) systems at 1173K. Master alloy Co-40 at.% Al (Co40Al) were prepared in a vacuum induction melting furnace using the high-purity Co (99.95%) and Al (99.95%). Then the obtained Co40Al ingot was homogenized at 1473K for 24 h, followed by quenching in ice water. Co40Al master alloy was used to replace pure Al to meet the high temperature requirement of diffusion annealing.

Schematic diagram of the designed diffusion multiples of Co-Al-X system is depicted in Fig. 1. All the ingots have a purity of at least 99.9% metals basis. All the surfaces of ingots were sanded with 1200 grit sandpapers and cleaned with ethanol in an ultrasonic bath to obtain flat and clean surfaces. The prepared Co40Al, Ti, Cr, Ni blocks were inserted into a high purity Ni cartridge with dimensions of 14 mm×14 mm×50 mm. Then the package was sealed into a Q235 low carbon steel sheath by manual arc welding. The wall thickness of the Ni cartridge is 3 mm to ensure the close contact between the metal blocks in the process of thermal isostatic pressure. After sealing, the high temperature hot-isostatic pressing treatment was performed on the whole encapsulation at 1423 K for 3 h with 120 MPa.

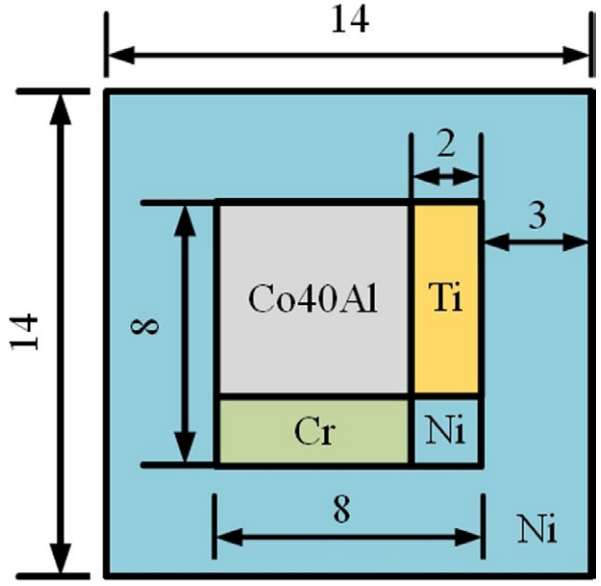

Fig. 1. Cross-sectional schematics of diffusion multiples of Co-Al-X (X = Ti, Cr, Ni) system (mm)

Subsequently, the sample was sealed in a quartz tube and put into a muffle furnace for diffusion annealing heat treatment at 1173 K for 1000 h, followed by water quenching. Finally, the obtained diffusion multiple samples with different interfaces were cut by wire cutter, and then a series of SiC papers from 600 to 2500 grit was used to polish the surfaces of the samples. Water-soluble diamond grinding paste with particle size of 1.5 μm was applied to mechanically polish until the whole polished surface was smooth and clean without any scratch. Phase compositions and surface morphologies of various diffusion interfaces were observed and analyzed by a ZEISS SUPRA 55 scanning electron microscopes (SEM) equipped with X-ray energy spectrometer (EDS).

Nano-indentation test with a maximum load of 5000 μN were performed to study the performance of diffusion layers, and the Nano Indenter G200 indentation device was employed. Before testing, the surfaces of the samples were ground on SiC papers from 320 to 3000 grit, polished for a mirror like surface and cleaned with ethanol in an ultrasonic bath to remove the residual stress caused by the mechanical grinding and polishing. Due to differences of diffusion behavior in the same layer and metal compositions in the region closed to matrix, two tested points were measured in Co40Al-Cr and Co40Al-Ti-Ni diffusion layers during nano-indentation test.

2.2. Basic calculations

The hardness and elastic modulus can be calculated using the data of nano indentation test. Oliver-Pharr method was carried out with the following equation defined the contact stiffness of materials as [25]:

$$S = \frac{dP}{dh} \tag{1}$$

where S is the contact stiffness of materials; P corresponds to the value of load; h is the value of displacement. The equivalent contact depth h_c can be calculated by elastic contact theory as given [25]:

$$h_{S_{\max}} = \frac{\varepsilon P_{\max}}{S} \tag{2}$$

$$h_c = h_{\max} - h_S \tag{3}$$

where h_s denotes the deflection of the surface in the vicinity of the contact and $h_{S_{\max}}$ is h_s at the peak load; ε is related to the shape of the head; $h_{\max}$ and $P_{\max}$ are maximum displacement and maximum load, respectively. The area of indentation contact projection A can be determined by Eq. (4) [25]:

$$A = 24.56h_c^2 \tag{4}$$

Then the hardness (H) and elastic modulus (E) can be calculated using Eqs. (5) and Eqs. (6, 7), respectively [25].

$$H = \frac{P_{\max}}{A} \tag{5}$$

$$E = \frac{E_i E_r (1-\nu^2)}{E_i - (1-\nu_i^2)E_r} \tag{6}$$

$$E_r = \frac{S\sqrt{\pi}}{2\beta\sqrt{A}} \tag{7}$$

where E_i and V_i are the elastic modulus and Poisson ratio of the head, for natural diamond head, E_i and V_i are 1114 GPa and 0.07, respectively. E_r is the reduced elastic modulus; ν is the Poisson ratio of the measured material; β is the constant associated with the geometry of the head.

3. Results

Fig. 2 shows the SEM image of Co40Al master alloy. It is found that Co40Al is comprised of Co matrix and homogeneously distributed β-CoAl precipitate. In Co40Al master alloy side, the region away from interfaces can be regarded as a matrix without significant changes in composition. The precipitation of β-CoAl plays a significantly role in strengthening the alloy [26]. This typical two-phase microstructure of Co40Al master alloy is beneficial to recognizing the initial location of the diffusion layer.

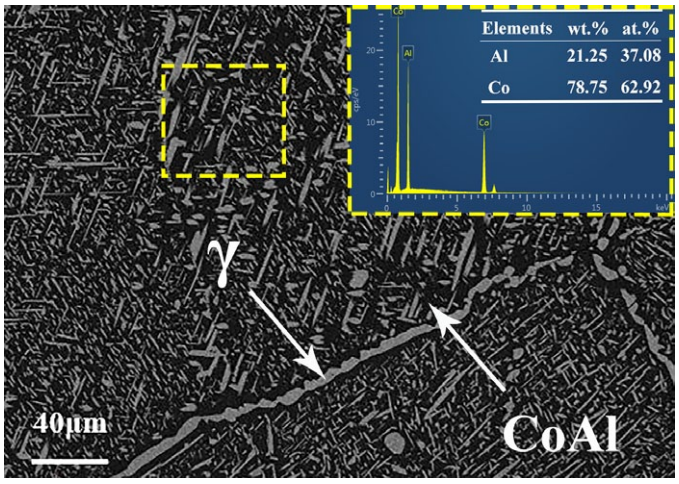

Fig. 2. SEM morphology of Co40Al master alloy

3.1. Diffusion interface and properties of Co-Al-Ni system

Fig. 3 displays the SEM micrographs and EDS line scanning results of Co-Al-Ni diffusion transition layers. Four diffusion layers with explicit phase boundaries can be distinguished along the diffusion region from Co40Al side to Ni side. Notably, it was difficult to recognize the interface between diffusion layer and Co40Al matrix, which is attributed to the near Co40Al matrix during diffusion annealing process. The precipitation of second phase was caused by the inter-diffusion of atoms between Co40Al and Ni matrixes, and resulted in the inconspicuous interface. Moreover, the double-phases microstructure of Co40Al matrix exhibited different resistance to the inward diffusion mobilities of Ni atoms. In addition, some sparse holes with linear distribution on the side of Ni matrix were observed. Such large size holes formed during diffusion annealing can be explained by the Kirkendall effect, the different diffusion coefficients of Co, Al and Ni atoms lead to the formation of vacancies flow in convective diffusion, thus leads to the formation of Kirkendall holes during diffusion annealing [27]. Besides, it might due to the different stresses induced by different thermal shrinkage or the cutting process for preparation of metallographic sample.

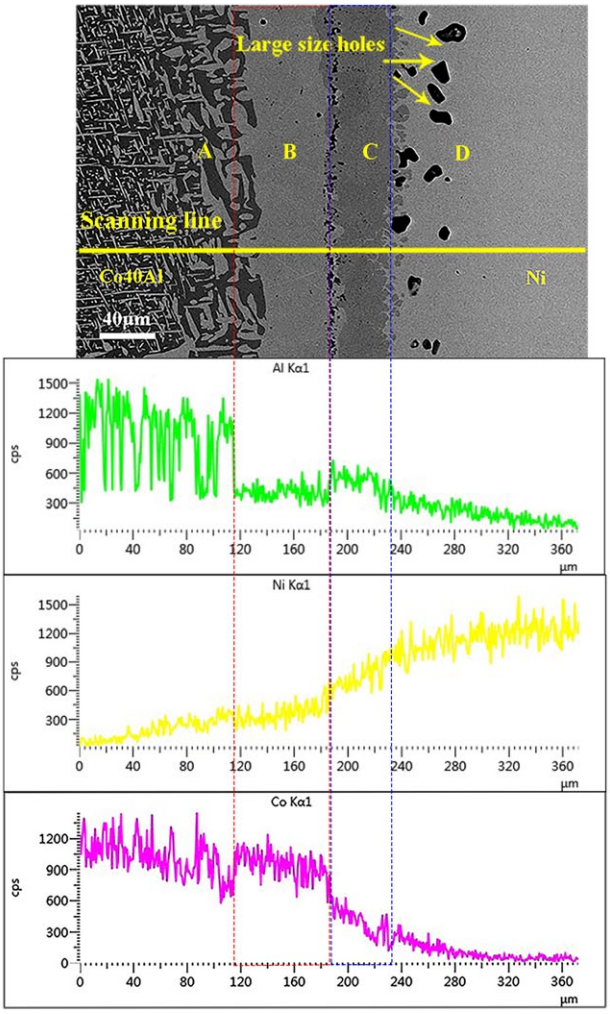

Fig. 3. SEM micrograph and element distributions of Co-Al-Ni diffusion interface

The element variation and distribution in the diffusion layers of Co-Al-Ni were determined by (EDS) line-scanning. As shown in Fig. 3, the diffusion layer of Co-Al-Ni was composed of four diffusion sublayers, which are marked as A, B, C and D from Co40Al matrix to Ni matrix. The intensities of Co, Al and Ni varied continuously in each diffusion sublayer, while an obvious jump occurred in the area near each sub-interface. Additionally, both the concentration of Co and Al elements decreased from Co40Al matrix to Ni matrix, while that of Ni element inversely increased. Violent oscillations of scanning intensities of Co and Al elements in region A can be obviously distinguished in Fig. 3, which was derived from the double-phases of Co40Al

matrix with scanning. Specifically, the concentration of Al element decreased firstly from Co40Al matrix to Ni matrix, then increased slightly, and subsequently decreased gradually. The increase of Al concentration in the sublayer connected with Ni matrix indicated that the migration of Al atoms was very fast in Co-Al-Ni interface. In this case, it also demonstrated that Al element preferentially diffused to form intermetallic compound with Ni element.

As shown in Fig. 4, element distributions along the diffusion interface from Co40Al side to Ni matrix were analyzed by scanning point by point with a distance of 20 μm. The obtained elemental compositions of sublayers A, B, C and D are shown in TABLE 1. Theoretically, the diffusion of alloying elements during annealing should be in a dynamic equilibrium, while the phase compositions in different regions vary with the change of alloying elements. The phase equilibrium of different tested points is calculated based on element compositions, and the calculated phase contents of points 7-12 in Fig. 4 are displayed in Fig. 5. From composition distribution, it can be seen that γ_{Co}

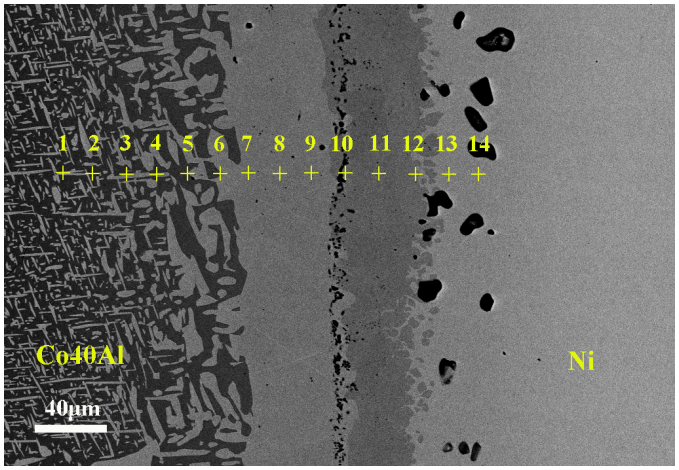

Fig. 4. EDS text points distributions of Co-Al-Ni diffusion interface

TABLE 1

Contents of Co, Al and Ni of sublayers A, B, C and D in Fig. 4, respectively (at. %)

Elements/ Sublayers	Text points	Co	Al	Ni	Phase
Sublayer A	1	59.08	35.91	5.01	$\beta + \gamma_{Co}$
	2	55.8	34.41	9.79	$\beta + \gamma_{Co}$
	3	53.29	33.61	13.1	$\beta + \gamma_{Co}$
	4	53.97	29.91	16.12	$\beta + \gamma_{Co}$
	5	50.25	29.04	20.71	$\beta + \gamma_{Co}$
	6	43.29	32.53	24.18	$\beta + \gamma_{Co}$
Sublayer B	7	65.75	13.12	21.13	γ_{Co}
	8	60.57	13.24	26.19	γ_{Co}
	9	54.42	13.14	32.44	γ_{Co}
Sublayer C	10	28.64	18.06	53.3	$\gamma + \gamma'$
	11	22.09	18.2	59.71	$\gamma + \gamma'$
	12	17.90	17.61	64.49	$\gamma + \gamma'$
Sublayer D	13	14.34	9.27	76.39	γ_{Ni}
	14	5.94	7.34	86.72	γ_{Ni}

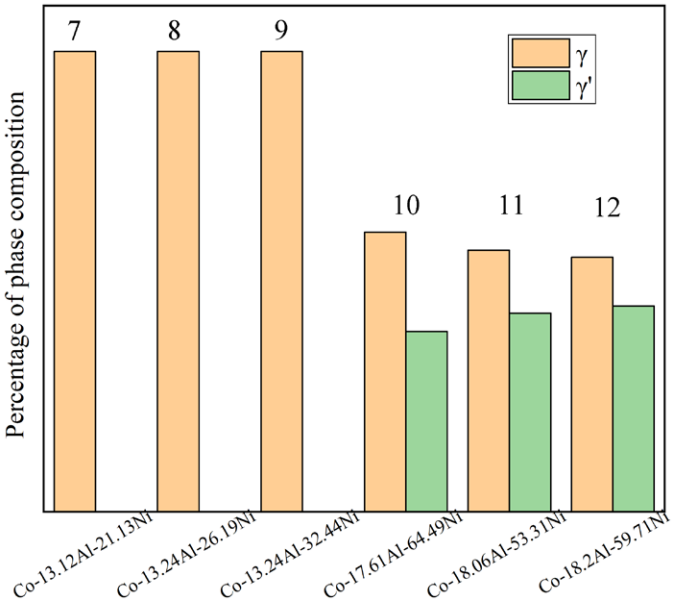

Fig. 5. Calculated phase content of the referred EDS test points in sublayers B and C used JMatpro

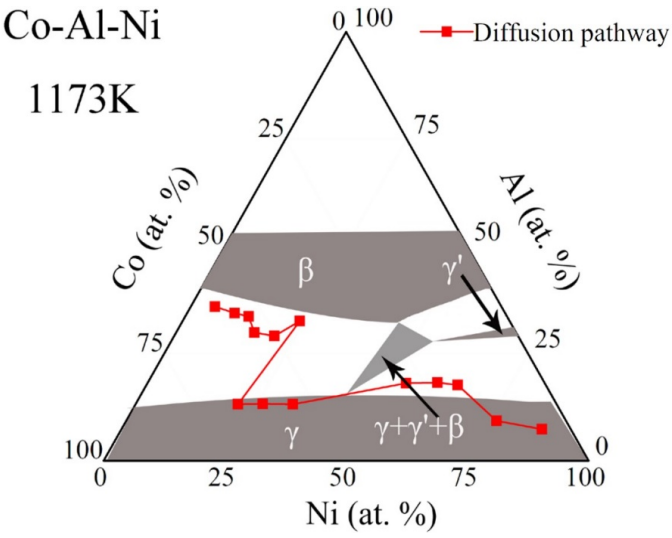

Fig. 6. Diffusion pathway of Co-Al-Ni interface at 1173K section

and $\gamma + \gamma'$ phases are in sublayers B and C, respectively. Moreover, the γ' content increases with area close to Ni matrix. Based on the variation of phase compositions, the diffusion pathway of Co-Al-Ni interface was determined and plotted in Co-Al-Ni isothermal section at 1173 K, as shown in Fig. 6. From the Co40Al side to the Ni side, the $\beta + \gamma_{Co}$, γ_{Co}, $\gamma + \gamma'$ and γ_{Ni} sublayer can be determined by comparing with the Co-Al-Ni ternary phase diagram at 1173K in reference [28].

It is well known that the variety of alloying elements and the diffusion layers affect the formation of intermetallic phases. In $\beta + \gamma_{Co}$ sublayer, from the side near Co40Al to the side near Ni, Co and Al contents decreased continuously, while Ni contents increased comparatively, which resulted in a continuous drop in fraction of β phase and the increase of γ_{Ni} phase. Moreover, the diffusion coefficient of Al decreased in sublayer with the

formation of γ_{Co} and γ_{Ni}. In $\gamma + \gamma'$ sublayer, a coexistence of γ'-Co_3Al and γ'-Ni_3Al can be expected due to the low content of Ni atoms. The large concentration gradient of Ni atoms along diffusion interfaces led to a continuous diffusion of Al atoms from Co40Al to Ni matrix, which directly resulted in the formation of γ'-Ni_3Al phase. Finally, the Co and Al content decreased gradually, and γ' phase converted to γ_{Ni} phase.

Fig. 7 shows the nano-indentation test performed on four diffusion regions in Co-Al-Ni interface. The selected test points are numbered as shown in Fig. 7a and the distance between each two test points was set as 30 μm. During testing process, the selection of tested points should avoid the holes areas because the test points near cracks or holes may cause collapse or annihilation for premature plastic deformation of the sample, resulting in abnormal low hardness and elastic modulus. This can be explained from the perspective of energy that the cracks or holes reduce the potential energy or strain energy in the collapse process. In this case, the bigger cracks lead to the higher reduction of the potential energy [29,30]. The load-displacement curves of different points are displayed in Fig. 7b. The displacement and the area enclosed by the curve represent the hardness and the elastic modulus, respectively. It can be seen that the load-displacement curves of the six measured points were similar in shape. The hardness and elastic modulus of each point were calculated and plotted in Fig. 7c. Combined with Fig. 7a, the minimum hardness value of 3.08 GPa was located in γ_{Co} sublayer, and the values of hardness became to be high with closing to $\gamma + \gamma'$ phase layer. Whereas, the elastic modulus changed dramatically in γ sublayer. The maximum value of 186.82 GPa appeared in γ_{Co} sublayer closed to Co40Al side, and the minimum value of 160.12 GPa was obtained in γ_{Ni} sublayer.

The element distributions and hardness variation as a function of distance derived from Co40Al side to Ni side along diffusion interface are displayed in Fig. 7d. It can be found that the hardness decreased with the decrease in β phase content in $\beta + \gamma_{Co}$ sublayer, while the hardness of $\gamma + \gamma'$ sublayer was higher than that of $\beta + \gamma_{Co}$ sublayer due to the existence of hard γ' phase. The increase in content of hard γ' phase resulted in the hardness improvement of diffusion layer. Furthermore, the hardness in $\gamma + \gamma'$ sublayer declined from Co40Al side to Ni side, indicating the continuous transformation from γ' phase to γ_{Ni} phase, which results in the appearance of the smallest hardness in γ_{Ni} sublayer.

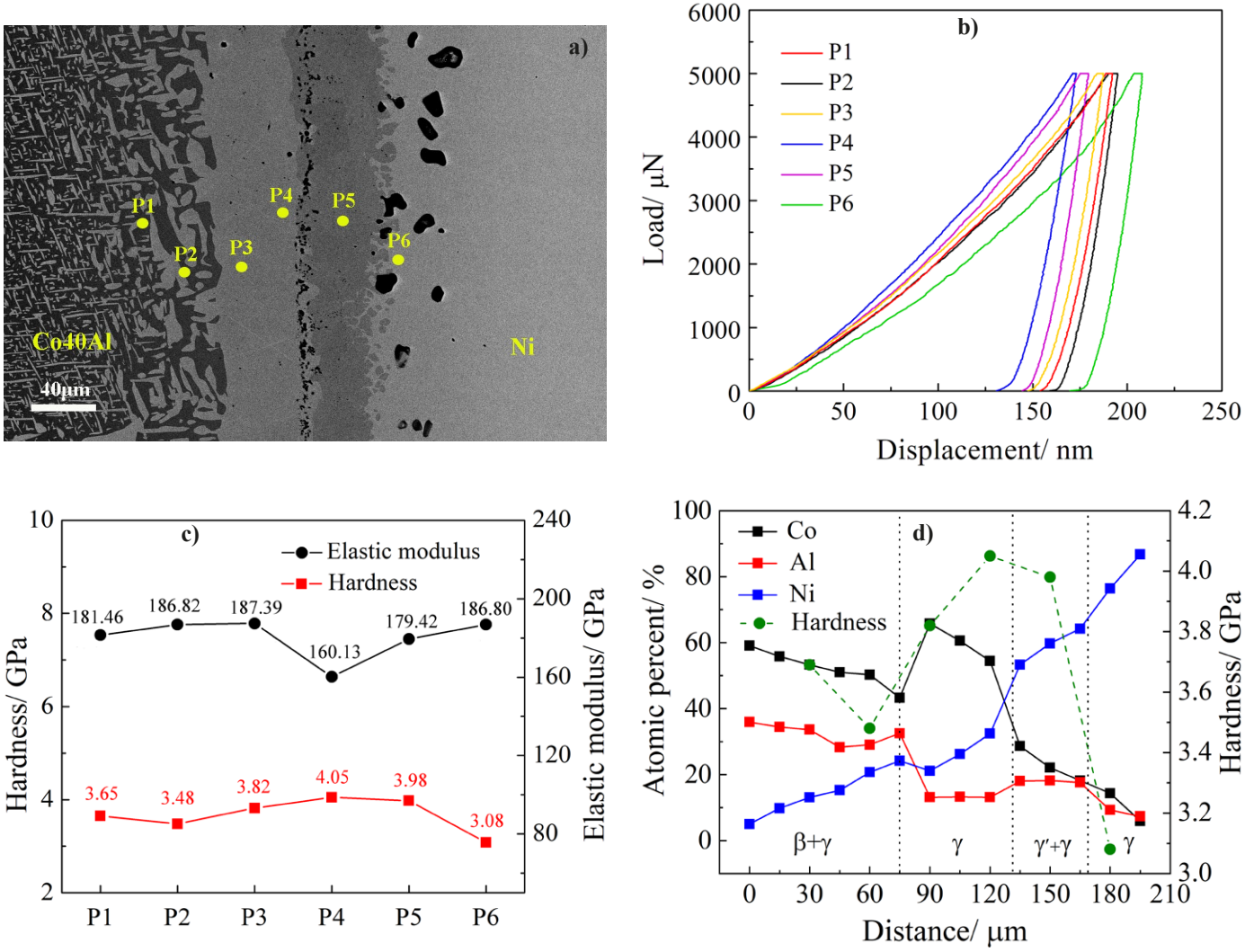

Fig. 7. (a) Location of the nano-indentation test points of Co-Al-Ni interface, (b) Load-displacement curves of six nano-indentation test points, (c) Hardness and elastic modulus of six nano-indentation test points, (d) Position-component-hardness curve of Co40Al-Ni diffusion layer

3.2. Diffusion interface and properties of Co-Al-Cr system

Fig. 8 displays the SEM micrographs and EDS line scanning results of Co-Al-Cr diffusion interface. Three diffusion layers with relatively homogeneous thickness as well as a crack appeared along the diffusion layer near Cr side. Three diffusion sublayers in Co-Al-Cr system were marked as E, F, and G from Co40Al matrix to Cr matrix. Among all sublayers, the thickness of middle diffusion layer was thinner than that of the other two layers. Furthermore, the concentration of Co, Al, and Cr element varied continuously in each diffusion sublayer, along with a sharp change appearing near the diffusion sublayer interface. In F sublayer, Cr content increased from Co40Al to Cr matrix, meanwhile Co and Al contents decreased, conversely.

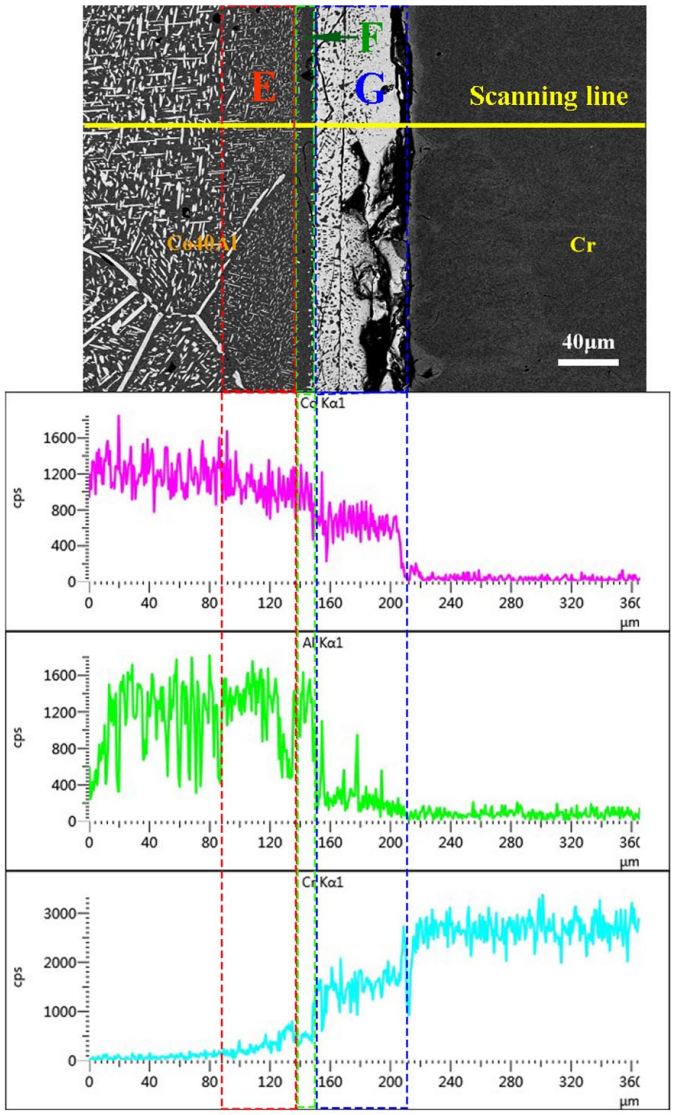

Fig. 8. SEM micrograph and elements distributions of Co-Al-Cr diffusion interface

Elements distributions along the diffusion interface from Co40Al to Cr matrix were analyzed by scanning point by point with a distance of 15 μm, and texted points are marked in Fig. 9.

The obtained elemental compositions of sublayers E, F and G are listed in TABLE 2. Based on the composition analysis, the phase equilibrium of different test points was calculated, and calculated phase contents of points 4-11 in Fig. 9 are displayed in Fig. 10. From composition distribution, it can be speculated that composed phases in sublayers E, F and G can be verified as $\delta+\beta+\gamma$ phases, single γ_{Co} phase and single σ phase, respectively, and accordingly diffusion pathway of Co-Al-Cr interface was obtained and plotted, as shown in Fig. 11.

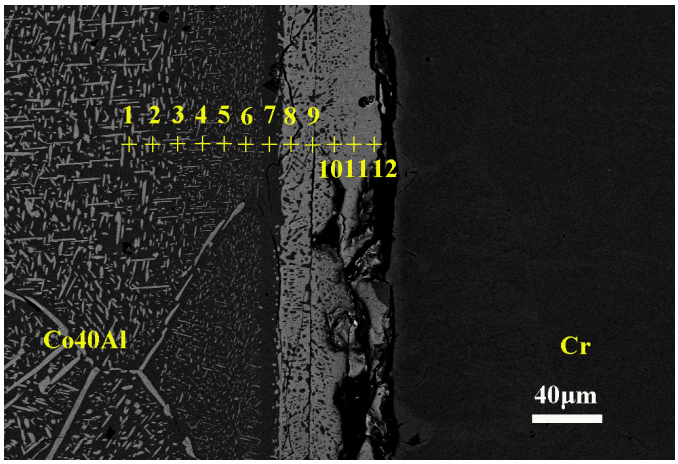

Fig. 9. EDS text points distribution of Co-Al-Cr diffusion interface

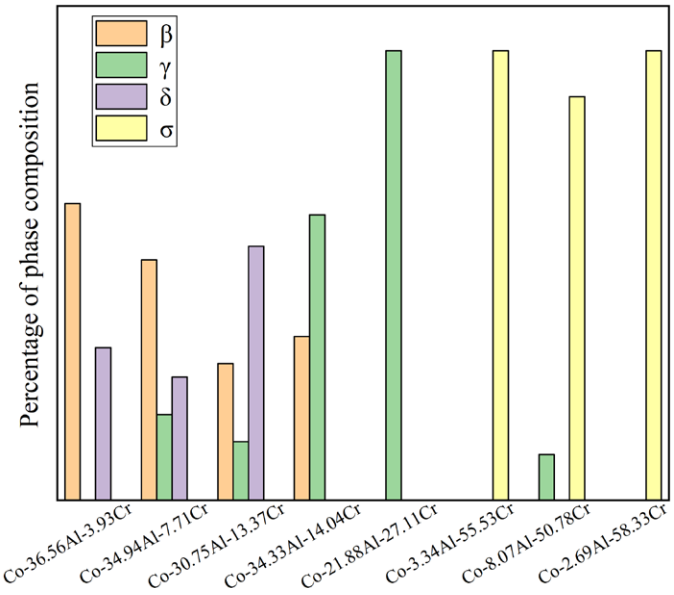

Fig. 10. Calculated phase content of the referred EDS test points in sublayers E, F and G

In E sublayer from Co40Al side to Cr side, Co and Al content decrease with Cr content increased slightly, and main phase was β-Co40Al. Cr content increased significantly in G sublayer, while the concentration variation of Co and Al was small. In this case, Cr content of mutations is presumably the main reason for the changes of the formed diffusion sublayer. Likewise, G sublayer exhibited the dramatic decrease in Al and Co contents but the sharp increase in Cr content. Notably, the

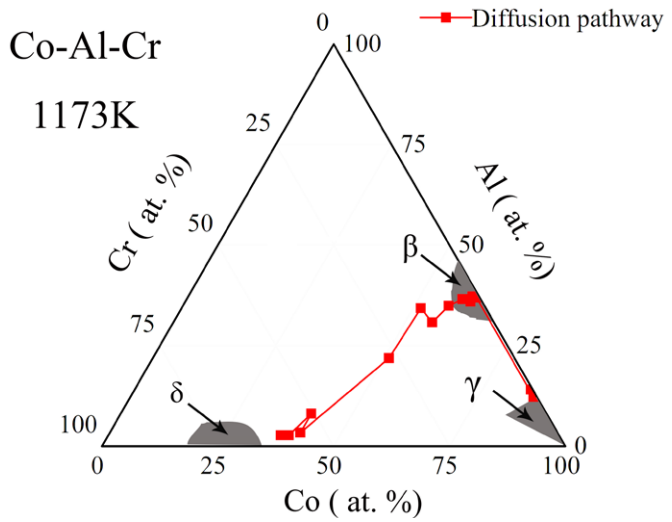

Fig. 11. Diffusion pathway of Co-Al-Cr interface at 1173K section

TABLE 2

Contents of Co, Al and Cr of sublayers E, F and G in Fig. 8, respectively (at. %)

Elements/ Sublayers	Text points	Co	Al	Cr	Phase
Sublayer E	1	62.35	36.93	0.72	$\delta+\beta+\gamma$
	2	61.32	37.21	1.47	$\delta+\beta+\gamma$
	3	61.58	35.91	2.51	$\delta+\beta+\gamma$
	4	59.51	36.56	3.93	$\delta+\beta+\gamma$
	5	57.35	34.94	7.71	$\delta+\beta+\gamma$
	6	55.88	30.75	13.37	$\delta+\beta+\gamma$
Sublayer F	7	51.63	34.33	14.04	$\beta+\gamma$
Sublayer G	8	51.01	21.88	27.11	γ
	9	41.13	3.34	55.53	σ
	10	41.15	8.07	50.78	σ
	11	38.98	2.69	58.33	σ
	12	37.26	2.68	60.06	σ

cracks could be observed in G sublayer, indicating σ phase with hard and crisp characteristics formed.

Fig. 12a shows the nano-indentation test performed on four diffusion sublayers in Co-Al-Cr interface. The load-displacement curves of different points are displayed in Fig. 12b. All the curves showed similar shapes. Notably, a larger displacement appeared at the tested point 7 near Co40Al matrix (Fig. 12a), which was ascribed to the large plastic deformation at this area

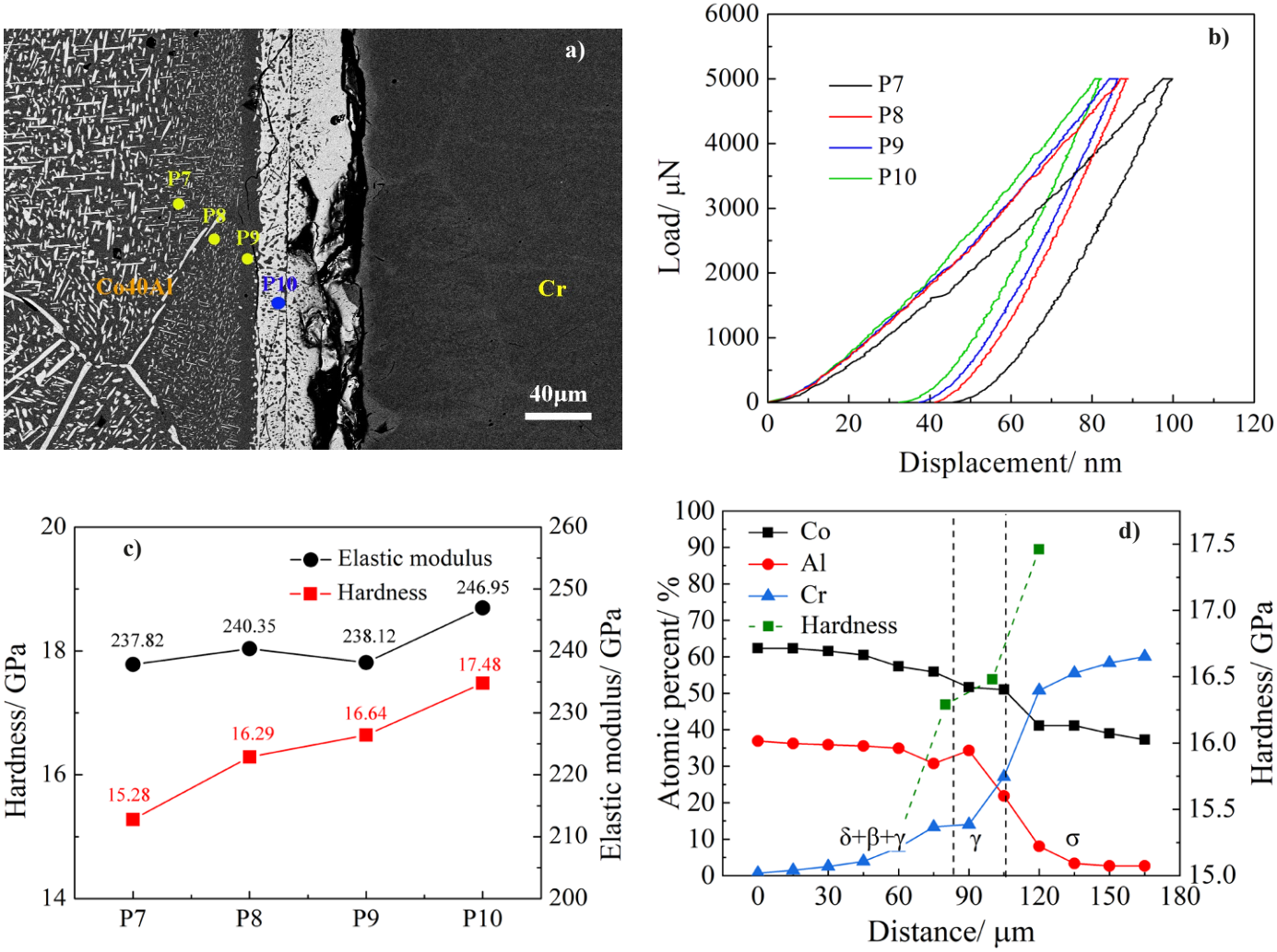

Fig. 12. (a) Location of the nano-indentation test point of Co-Al-Cr interface, (b) The load-displacement curves of four nano-indentation test points, (c) The hardness and elastic modulus of four nano-indentation test points, (d) Position-component-hardness curve of Co-Al-Cr diffusion layer

during hot-compression stage. The hardness and elastic modulus of four text points were calculated and plotted in Fig. 12c. The minimum hardness was 15.28 GPa located in $\delta+\beta+\gamma$ sublayer, while σ sublayer possessed the maximum hardness yielding 17.48 GPa. Conversely, the elastic modulus in $\delta+\beta+\gamma$ sublayer and σ sublayer exhibited a minimum (237.82 GPa) and a maximum (246.96 GPa), respectively.

The elements distributions and variety of hardness as a function of distance derived from Co40Al side to Cr side along diffusion interface are displayed in Fig. 12d. It can be found that both elements distributions and hardness were positively related to Cr content.

3.3. Diffusion interface and properties of Co-Al-Ti system

Fig. 13a represents SEM micrograph and EDS line scan results of Co-Al-Ti diffusion interface. In contrast to diffusion interface in above alloy system, only one diffusion layer penetrated from Co40Al side to Ti side can be recognized in Co-Al-Ti system, and no Ti matrix can be found. Interestingly, the concentration of Co and Al elements was very low in the diffusion layer, which can be attributed to low solubility of Co and Al in Ti matrix resulting in a small amount of Co and Al diffusing to the middle diffusion layer. Whereas, content of Ni element was relatively high in the middle diffusion layer, demonstrating that the middle diffusion layer was mainly composed of diffused Ni and Ti. As a result, diffusion sublayer was mainly formed by $TiNi_X$ intermetallic phase. Such Ti element abnormal diffusion probably caused by easy absorption of impurity elements (Ni) easily during phase transition. In addition, generation of other metastable phases may also lead to abnormal diffusion [31].

From EDS line scanning results from Co40Al side to Ti side, Co and Al elements content decreased, while Ni element amount increased. It can be inferred the middle diffusion layer was similar to Co40Al matrix and exhibited double-phases structure. Element distributions were investigated using EDS along the diffusion interface. The content range of Ti element and Ni element was 22.2-37.3 at.% and 40.06-69.41 at.%, respectively. Such high Ni content might derive from the formation of $TiNi_X$ intermetallic phase. This phenomenon of phase deficiency may be caused by low diffusion annealing temperature.

The load-displacement curves of the diffusion sublayer are shown in Fig. 13b. It can be seen that load-displacement curves of two measured points were similar in shape. In addition, hardness and elastic modulus of each point were calculated and also listed in TABLE 3. Both hardness and elastic modulus of the location close to Ti matrix were higher than that close to Co40Al side.

Comparing the properties of the three diffusion interfaces, mechanical performance of Co-Al-Ti diffusion interface is better than that of Co-Al-Ni interface, but worse than that of Co-Al-Cr interface. To be detailed, the elastic modulus of Co-Al-Cr diffusion layer were 35% and 12% higher than that of Co-Al-Ni and

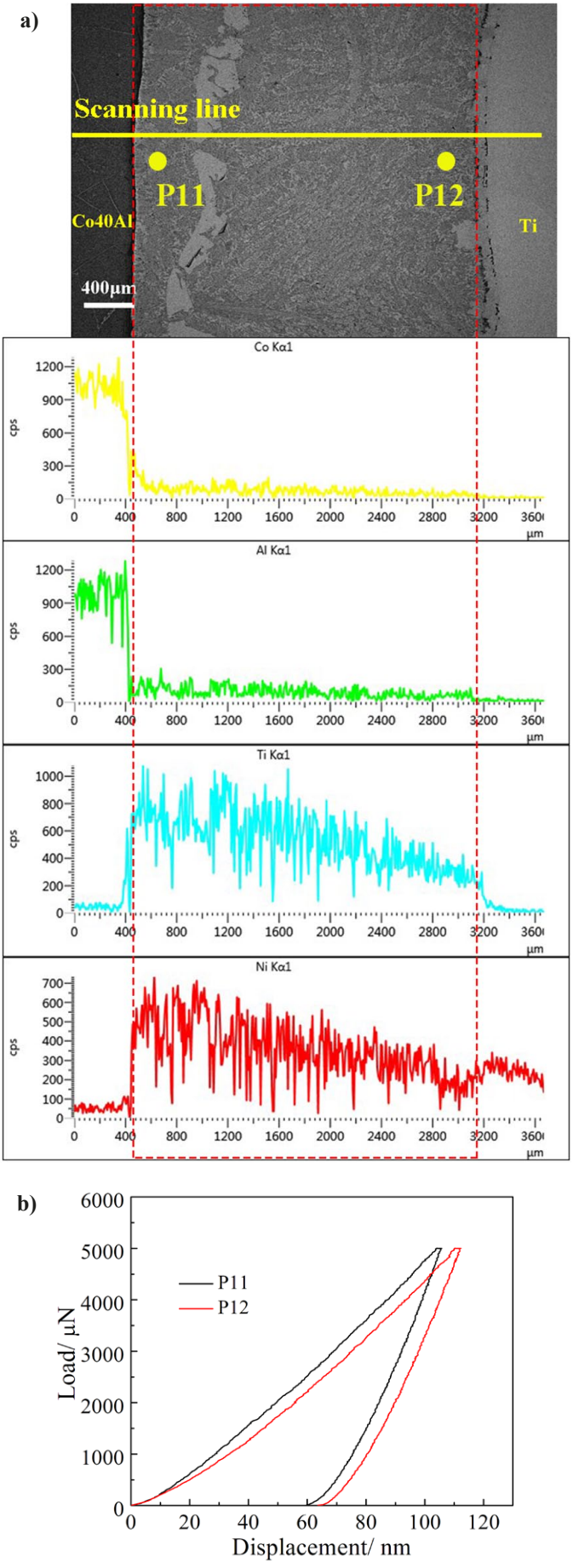

Fig. 13. (a) Element distributions of Co-Al-Ti diffusion interface; (b) Load-displacement curves of two nano-indentation tested points

TABLE 3

Summary data of the hardness (*H*), elastic modulus (*Er*) of nano-indentation text points. (1~6 represent the data of Co-Al-Ni system, and 7~10 represent the data of Co-Al-Cr system, and 10,11 represent the data of Co-Al-Ti system)

Text points	Interface	Location	*Er* (GPa)	*H* (GPa)
p1	Co-Al-Ni	$\beta+\gamma$	181.46	3.65
p2			186.82	3.48
p3		γ	187.39	3.82
p4			160.13	4.05
p5		$\gamma+\gamma'$	179.42	3.98
p6		γ	186.80	3.08
p7	Co-Al-Cr	$\delta+\beta+\gamma$	237.82	15.28
p8			240.35	16.29
p9		γ	238.12	16.64
p10		σ	246.95	17.48
p11	Co-Al-Ti	Near Co40Al side	205.21	10.91
p12		Near the Ti side	213.26	11.21

Co-Al-Ti interface, respectively. However, high hardness of Co-Al-Cr interface limited large scale applications in engineering. The $\gamma+\gamma'$ sublayer in Co-Al-Ni interface and γ + $TiNi_X$ sublayer in Co-Al-Ti interface displayed better mechanical properties. In order to meet the dual requirements of elasticity and hardness, Co-Al-Ti-Ni system was chosen as our research target.

4. Discussion

4.1. Diffusion ability and partition of elements

4.1.1. Evaluation of diffusivity

To estimate the mutual diffusion coefficient of binary or ternary alloys with incomplete data, Fick's first law was applied. In general, when diffusion occurs in diffusion multiple, the diffusion fluxes in the diffusion pair consists of two parts: the pure atomic diffusion and the fluxes generated by the whole lattice movement, and the movement of the lattice can be ignored.

The total diffusion flux of i component $(J_i)_T$ can be expressed as Eqs. (8) and (9) follows [32].

$$(J_A)_T = C_A V = -D_A \frac{\partial C_A}{\partial x} \tag{8}$$

$$(J_B)_T = C_B V = -D_B \frac{\partial C_B}{\partial x} \tag{9}$$

where C_A, C_B are the volume concentration of element A and B, respectively; V denotes the rate of atomic diffusion; D_A, D_B are the self-diffusion coefficient of element A and B, respectively. If there are only two components in the diffusion1 multiple, the following relationship exists as shown in Eq. (10):

$$\frac{C_A}{C_B} = \frac{X_A}{X_B} \tag{10}$$

where X_A, X_B are molarity of element A and B, respectively. If the molarity is a constant, the following equations can be drawn [33]:

$$(J_A)_T = -(J_B)_T \tag{11}$$

$$V_A = (D_A - D_B)\frac{\partial X_B}{\partial X} \tag{12}$$

$$(J_A)_T = -(D_A X_B + D_B X_A)\frac{\partial C_A}{\partial x} = -\overline{D}\frac{\partial C_A}{\partial x} \tag{13}$$

$$(J_B)_T = -(D_A X_B + D_B X_A)\frac{\partial C_B}{\partial x} = -\overline{D}\frac{\partial C_B}{\partial x} \tag{14}$$

$$\overline{D} = D_A X_B + D_B X_A \tag{15}$$

The self-diffusion coefficient of the atom D_i can be calculated by the following Eqs. (16-18) [34]:

$$D_i = D_{0i}\exp\left(-\frac{Q_i}{RT}\right) \tag{16}$$

$$Q_i = RT_m(K + 1.5V_i) \tag{17}$$

$$D_{0i} = \frac{Q_i a_i^2}{N_A h} \tag{18}$$

where D_0 is a frequency factor; Q denotes the diffusion activation energy, K is the factor associated with the lattice, the value is 15.5 when the lattice is FCC and HCP [35]. V denotes the valence of element, the values are 3, 2.8, 2.5, for the elements in VB group (Ti, Al), VIB group (Cr, W, Mo), VIII group (Co, Ni), respectively [36]. T_m is the melting point of a metal; A is the lattice constant; N_A stands for Avogadro's constant; h is the Planck constant.

To more intuitively illustrate the diffusion ability of Al, Cr and Ni elements, the following data were selected in the phase region close to binary components for calculation using Eq. (15), calculated data of frequency factor D_0 and diffusion activation energy Q are shown in TABLE 4, and the results of inter-diffusion coefficients are listed in TABLE 5.

TABLE 4

Calculation of D_0 and Q of different element

Element	*Q* (kJ/mol)	D_0
Co	282.96	8.80×10^{-5}
Al	155.13	6.39×10^{-5}
Ni	276.24	8.59×10^{-5}
Cr	348.86	7.41×10^{-5}

TABLE 5

Calculation of inter-diffusion coefficients of different phases

Phase	Calculation point	Self-diffusion coefficient		Inter-diffusivity
β-Co40Al	$Co_{62.92}Al_{37.08}$	$\tilde{D}^{Co}_{AlAl}$	1.32×10^{-15}	2.254×10^{-15}
γ(Co, Ni)	$Co_{5.94}Ni_{86.70}$	$\tilde{D}^{Co}_{NiNi}$	3.75×10^{-15}	3.551×10^{-15}
δ	$Co_{37.26}Cr_{60.08}$	$\tilde{D}^{Co}_{CrCr}$	2.10×10^{-15}	3.085×10^{-15}

According to the results, the diffusion coefficient of Ni atom is highest, and that of Cr atom is the weakest (except for the Al element). TABLE 6 lists the thickness of each sublayer of Co-Al-Ni interface and Co-Al-Cr interface, respectively. The thickness of the Co-Al-Cr diffusion layer is the smallest because energy required for the diffusion of Cr atom is the highest.

TABLE 6

Summary data of the thickness of sublayers about Co-Al-Ni interface and Co-Al-Cr interface

Sublayers	Interface	Phase	Thickness (μm)
A	Co-Al-Ni	$\beta + \gamma_{Co}$	40.53
B		γ_{Co}	72.18
C		$\gamma + \gamma'$	44.17
D		γ_{Co}	33.12
E	Co-Al-Cr	$\delta + \beta + \gamma$	47.52
F		γ	18.20
G		σ	54.28

4.1.2. Elements partitioning

The researchers have studied the isothermal section of Co40Al-Ni system at 1173 K. Compared to other studies [27], the sublayer of $\beta + \gamma$, γ, $\gamma + \gamma'$ agree well with the tie-lines obtained by them.

Previous studies have shown that Ni element can stabilize γ' phase. The addition of Co to Ni-based superalloys can increase the volume fraction since Co reduces the solubility of Al in γ phase [11]. In D sublayer, Ni content is higher than Co, which increase the tendency to form γ'-Ni_3Al phase. In addition, Co and Ni do not form binary phases [9], so the γ' of $\gamma + \gamma'$ sublayer is consist of more Ni_3Al but less Co_3Al. Similarly, the addition of Ni has the same effect to Co40Al, where Ni and Al react in solution to form γ'-Ni_3Al. According to the data of this experiment, in $\gamma + \gamma'$ sublayer, the ratio of Ni to Al atomic molar is closed to 3:1, which is well in agreement with our previous speculation. In $\gamma + \gamma'$ sublayer, the Ni content continued to increase, meanwhile the Al content remained almost unchanged. Llewelyn et al. [11] found that the selective distribution of Al to γ' phase in the alloy gradually increased with the increase in Co content in the alloy, and the maximum distribution range is about 19 at.%. In our work, the Co content of the $\gamma + \gamma'$ sublayer is around 20 at.%, which is similar to the previous report [27].

4.2. Comparison of mechanical properties

The hardness of Co-Al-Cr diffusion layer is significantly higher than other diffusion layers. In Co-Al-Ni system, in $\beta + \gamma_{Co}$ sublayer, the increasing of Ni occupied Al elements, leads to the

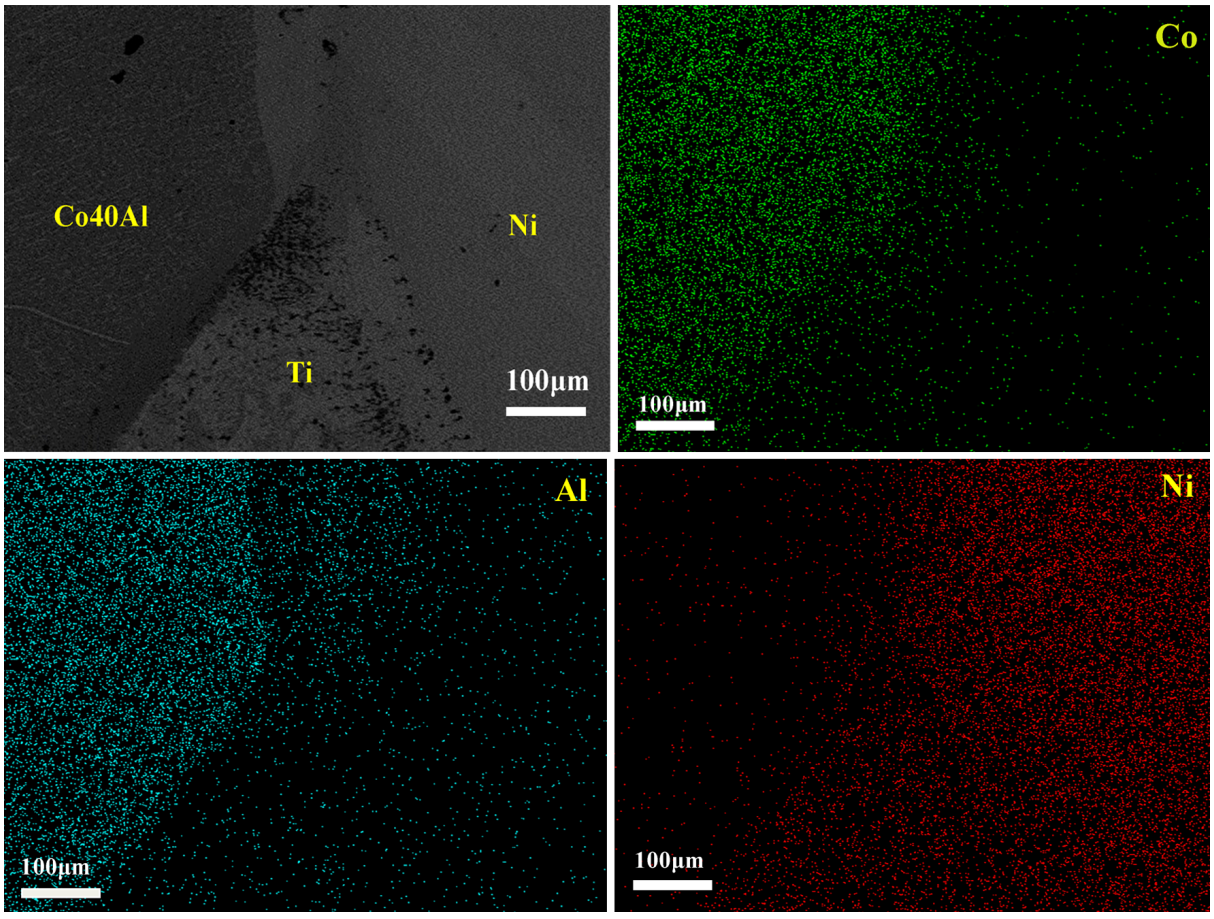

Fig. 14. Alloying elements distributions of Co-Al-Ti-Ni quaternary interface

hardness drop in the diffusion layer as the content of hard brittle β phase rising. In γ_{Co} sublayer, as a result of the gradual formation of γ' phase, the hardness of γ_{Co} is higher than $\beta + \gamma$ sublayer. In addition, the γ_{Ni} sublayer has the lowest hardness because of inexistence of γ' phase or β phase. Based on the above analysis, the hardness of each phase is ordered as $\gamma' > \gamma_{Co} > \beta > \gamma_{Ni}$.

Solution strengthening is the main reason of the hardness improvement, in addition, the high hardness of σ phase is due to the significant hardness of Cr itself, from $\delta + \beta + \gamma$ side to σ side, there is a positive correlation between the hardness of diffusion sublayer and Cr content, Co and Ni are the opposite. According to the experiment data, although Co-Al-Cr system has the best hardness, the high Cr content will bring bad effects on the properties of the novel Co-based superalloys [7,26].

Zhang et al. [37] proposed a general hypothesis that higher compositional complexity of FCC solid solution can increase the hardness of microstructure. However, Popp et al. [38] reported that the hardest phase is not necessarily the one with the most complex composition, and the microstructure of the sample with the best hardness did not occur at the greatest atomic mismatch and the elastic modulus mismatch might affect the hardness of microstructure. The factors affecting the hardness need to be further studied in the future.

5. Conclusions

The diffusion morphology and isothermal section of Co-Al-X system at 1173K were investigated using diffusion multiple approach. Extensive measurement of hardness and elastic modulus of the diffusion layers were performed by nano-indentation test. The diffusion ability of elements was evaluated by using the Darken equation.

(i) There were three diffusion sublayers in Co-Al-Ni system, including β-CoAl + γ_{Co}, γ_{Co}, $\gamma + \gamma'$-Ni_3Al, γ_{Ni}. The hardness of $\gamma + \gamma'$ sublayer were increased by up to 12 % compared with γ sublayer. The contents of Co, Ni and Al were 50-66 at.%, 24-34 at.% and 10-16 at.%, respectively, which can be used as a data reference for alloy design.

(ii) Three diffusion layers including $\delta + \beta + \gamma$, γ and σ phases were found in Co-Al-Cr system. The hardness was positively correlated with Cr element. However, the harmful brittle phase may be formed in δ region, which should be avoided when designing the alloys. Conversely, the difference of elastic modulus of each diffusion region is less than 5%. Due to the narrow size of each diffusion region, the addition amount of Cr element should be precisely controlled in alloy design.

(iii) There was only one diffusion layer (γ + $TiNi_X$) with a large value of thickness in Co-Al-Ti system. The microstructure hardness and elastic modulus at the Co-Al-Ti diffusion interface are moderate. Through the observation of the four-element joint, it can be found that the atomic mobility of Ni to Ti is stronger than that of Ni to Co40Al.

(iv) The diffusion coefficient of elements in the pseudo-binary system was evaluated by using the Darken equation, and the diffusion coefficient of different alloy elements in the Co matrix was Al > Ni > Cr.

Declaration of competing interest

We declare that we do not have any commercial or associative interest that represents a conflict of interest in connection with the work submitted.

Acknowledgements

The grants and financial supports from the National Natural Science Foundation of China and Shanghai Baosteel Group Company (Grant No. U1960204), the National Natural Science Foundation of China (Grant No. 51871042) and the Fundamental Research Funds for the Central Universities (Grant No. N2023026) are gratefully acknowledged.

REFERENCES

[1] J.C. Zhao, X. Zheng, D.G. Cahill, Mater. Today **8** (10), 28-37 (2005). DOI: https://doi.org/10.1016/s1369-7021(05)71122-6

[2] Y. Yuan, T. Chen, D. Li, U. Gerhards, F. Pan, H. Seifert, N. Moelans, Calphad **64**, 149-159 (2019). DOI: https://doi.org/10.1016/j.calphad.2018.12.005

[3] R. Xin, M. Wang, X. Huang, C. Guo, Q. Liu, Mater. Sci. Eng. A **596**, 41-44 (2014). DOI: https://doi.org/10.1016/j.msea.2013.12.030

[4] V.V. Shastry, V.D. Divya, M.A. Azeem, A. Paul, D. Dye, U. Ramamurty, Acta Mater. **61** (15), 5735-5742 (2013). DOI: https://doi.org/10.1016/j.actamat.2013.06.017

[5] J. Sato, T. Omori, K. Oikawa, I. Ohnuma, R. Kainuma, K. Ishida, Science **312** (5770), 90-91 (2006). DOI: https://doi.org/10.1126/science.1121738

[6] D. Migas, M. Kierat, G. Moskal, Arch. Metall. Mater. **66** (1), 5-14 (2021). DOI: https://doi.org/10.24425/amm.2021.134752

[7] T. Omori, K. Oikawa, J. Sato, I. Ohnuma, U.R. Kattner, R. Kainuma, K. Ishida, Intermetallics **32**, 274-283 (2013). DOI: https://doi.org/10.1016/j.intermet.2012.07.033

[8] C.H. Zenk, I. Povstugar, R. Li, F. Rinaldi, S. Neumeier, D. Raabe, M. Göken, Acta Mater. **135**, 244-251 (2017). DOI: https://doi.org/10.1016/j.actamat.2017.06.024

[9] Y. Yuan, L. Yang, D. Li, A. Tang, F. Pan, H. Seifert, N. Moelans, Calphad **63**, 156-163 (2018). DOI: https://doi.org/10.1016/j.calphad.2018.09.007

[10] Y. Zhuang, W. Liu, P. Xing, F. Wang, J. He, Acta Metall. Sin. (Engl. Lett.) **25** (2), 124-130 (2012). DOI: https://doi.org/10.11890/1006-7191-122-124

[11] S.C.H. Llewelyn, K.A. Christofidou, V.J. Araullo-Peters, N.G. Jones, M.C. Hardy, E.A. Marquis, H.J. Stone, Acta Mater. **131**, 296-304 (2017). DOI: https://doi.org/10.1016/j.actamat.2017.03.067

[12] Y. Zhang, Q. Wang, H.-G. Dong, C. Dong, H.-Y. Zhang, X.-F. Sun, Acta Metall. Sin. (Engl. Lett.) **31** (2), 127-133 (2018). DOI: https://doi.org/10.1007/s40195-017-0678-0

[13] S. Kobayashi, Y. Tsukamoto, T. Takasugi, Intermetallics **19** (12), 1908-1912 (2011). DOI: https://doi.org/10.1016/j.intermet.2011.08.004

[14] F. Xue, H.J. Zhou, X.F. Ding, M.L. Wang, Q. Feng, Mater. Lett. **112**, 215-218 (2013). DOI: https://doi.org/10.1016/j.matlet.2013.09.023

[15] I. Povstugar, P.-P. Choi, S. Neumeier, A. Bauer, C.H. Zenk, M. Göken, D. Raabe, Acta Mater. **78**, 78-85 (2014). DOI: https://doi.org/10.1016/j.actamat.2014.06.020

[16] Z. Chen, T. Dong, W. Qu, Y. Ru, H. Zhang, Y. Pei, S. Gong, S. Li, Corros. Sci. **156**, 161-170 (2019). DOI: https://doi.org/10.1016/j.corsci.2019.05.001

[17] Q. Gao, X. Dong, C. Li, Z. Lin, X. Yang, M. Dai, J. Alloy. Compd. **651**, 537-543 (2015). DOI: https://doi.org/10.1016/j.jallcom.2015.08.141

[18] Y. Jiang, Q. Gao, H. Zhang, X. Zhang, H. Li, Z. Liu, C. Liu, Mater. Sci. Eng., A **748**, 161-172 (2019). DOI: https://doi.org/10.1016/j.msea.2019.01.087

[19] X.F. Yao, J.P. Wei, Y.K. Lv, T.Y. Li, Acta Metall. Sin. **56** (5), 769-775 (2020). DOI: https://doi.org/10.11900/0412.1961.2019.00330

[20] Q. Gao, H. Zhang, H. Li, X. Zhang, F. Qu, Y. Jiang, Z. Liu, C. Jiang, J. Mater. Sci. **54** (11), 8760-8777 (2019). DOI: https://doi.org/10.1007/s10853-019-03513-9

[21] Q. Gao, C. Wang, F. Qu, Y. Wang, Z. Qiao, J. Alloy. Compd. **610**, 322-330 (2014). DOI: https://doi.org/10.1016/j.jallcom.2014.05.060

[22] Q. Gao, Z. Liu, H. Li, H. Zhang, C. Jiang, A. Hao, F. Qu, X. Lin, J. Mater. Sci. Technol. **68**, 91-102 (2021). DOI: https://doi.org/10.1016/j.jmst.2020.08.013

[23] P. Yang, C. Liu, Q. Guo, Y. Liu, J. Mater. Sci. Technol. **72**, 162-171 (2021). DOI: https://doi.org/10.1016/j.jmst.2020.09.024

[24] Q. Gao, Y. Jiang, Z. Liu, H. Zhang, C. Jiang, X. Zhang, H. Li, Mater. Sci. Eng., A **779**, 139139 (2020). DOI: https://doi.org/10.1016/j.msea.2020.139139

[25] Y. Takehara, H. Fujiwara, H. Miyamoto, Corros. Sci. **77**, 171-175 (2013). DOI: https://doi.org/10.1016/j.corsci.2013.07.042

[26] Q. Gao, F. Qu, H. Zhang, Q. Huo, J. Mater. Res. **31** (12), 1732-1740 (2016). DOI: https://doi.org/10.1557/jmr.2016.178

[27] L. Zhu, C. Wei, H. Qi, L. Jiang, Z. Jin, J.-C. Zhao, J. Alloy. Compd. **691**, 110-118 (2017). DOI: https://doi.org/10.1016/j.jallcom.2016.08.210

[28] R. Kainuma, M. Ise, C.C. Jia, H. Ohtani, K. Ishida, Intermetallics **4**, S151-S158 (1996). DOI: https://doi.org/10.1016/0966-9795(96)00034-9

[29] Z. Qian, J. Risan, B. Stadnick, G.B. McKenna, J. Polym. Sci., Part B: Polym. Phys. **56** (5), 414-428 (2018). DOI: https://doi.org/10.1002/polb.24554

[30] S. Gebhard, F. Pyczak, M. Goeken, Mater. Sci. Eng., A **523** (1-2), 235-241 (2009). DOI: https://doi.org/10.1016/j.msea.2009.05.068

[31] H. Bulou, J.P. Bucher, Phys. Rev. Lett. **96** (7), (2006). DOI: https://doi.org/10.1103/PhysRevLett.96.076102

[32] J. Chen, Y. Liu, G. Sheng, F. Lei, Z. Kang, J. Alloy. Compd. **621**, 428-433 (2015). DOI: https://doi.org/10.1016/j.jallcom.2014.09.139

[33] Z.C. Cordero, B.E. Knight, C.A. Schuh, Inter. Mater. Rev. **61** (8), 495-512 (2016). DOI: https://doi.org/10.1080/09506608.2016.1191808

[34] J. Askill, Empirical and Semi-Empirical Diffusion Relations, Springer US, Boston, MA (1970).

[35] S. Dushman, The diffusion coefficient in solid and its temperature coefficient, in: C.G. Suits (Ed), Structure of Matter, Pergamon, Oxford (1961).

[36] J.J. Han, C.P. Wang, X.J. Liu, J. Phase Equilib. Diffus. **34** (1), 17-24 (2013). DOI: https://doi.org/10.1007/s11669-012-0185-y

[37] Y. Zhang, T.T. Zuo, Z. Tang, M.C. Gao, K.A. Dahmen, P.K. Liaw, Z.P. Lu, Prog. Mater. Sci. **61**, 1-93 (2014). DOI: https://doi.org/10.1016/j.pmatsci.2013.10.001

[38] R. Popp, S. Haas, F. Scherm, A. Redermeier, E. Povoden-Karadeniz, T. Göhler, U. Glatzel, J. Alloy. Compd. **788**, 67-74 (2019). DOI: https://doi.org/10.1016/j.jallcom.2019.01.329